Altitude resolved ice-fraction in the uppermost tropical troposphere

M. Ekström[1] and P. Eriksson[1]

Received 15 April 2008; accepted 12 June 2008; published 15 July 2008.

[1] The exact nature of the processes responsible for the moistening of the upper tropical troposphere is still uncertain. Altitude resolved measurements of water vapor from Aura/Microwave Limb Sounder (MLS) and cloud ice from CloudSat are used to investigate the ratio of ice mass to total water. Horizontal and vertical ice-fraction distributions in the pressure range 100–316 hPa over the tropical region are presented. They reveal that the ice-fraction is generally low, less than 10% around 316 hPa in general and outside regions of deep convection in the altitude levels above. On the other hand, the ice-fraction can be significant at higher altitudes in large regions above deep convection, reaching values of ∼90%. Below the tropical tropopause layer (TTL) ice and water vapor distributions have similar spatial patterns indicating that water in both phases is transported up to the upper troposphere by the same processes. Over regions of strong deep convection where ice is transported into the TTL, the dissimilar patterns of ice and water vapor could be interpreted as that the cloud ice gives a limited final moistening effect. **Citation:** Ekström, M., and P. Eriksson (2008), Altitude resolved ice-fraction in the uppermost tropical troposphere, *Geophys. Res. Lett.*, *35*, L13822, doi:10.1029/2008GL034305.

1. Introduction

[2] Water in the upper troposphere (UT) and lower stratosphere (LS) plays an important role in several aspects of the Earth's climate. Tropospheric water vapor is the dominant green-house gas. Cloud particles attenuate upwelling longwave radiation and at the same time reflect incoming solar radiation. The net radiative effect depends on the altitude and composition of the cloud. Above the troposphere, stratospheric moisture enhances ozone reduction rates and is important in the stratospheric radiative balance.

[3] Accurate studies of the climatological and dynamic properties of water require an understanding of the mechanisms that transport water into the UT/LS region. In the tropics the convectively controlled UT and the radiatively controlled LS meet in a transition region, the tropical tropopause layer (TTL). In this region air is dehydrated before entering the LS. The exact processes behind the dehydration are still uncertain, but recent studies lean toward a combination of convective overshooting and slow ascent [e.g., *Webster and Heymsfield*, 2003; *Lelieveld et al.*, 2007]. The occurrence and distribution of cirrus clouds are important signatures of the ongoing processes. Here the lower boundary of the TTL is, loosely, defined around 14 km or 150 hPa.

[4] The outgoing longwave radiation in the tropics is most sensitive to water vapor in the region from the ground up to around 12 km [*Buehler et al.*, 2006]. In this context the transport of water to the UT is important, for example with respect to feedback mechanisms in a changing climate. A high correlation between cloud ice, i.e. ice water path (IWP), and upper tropospheric water vapor (UTWV) has been interpreted as moisture being transported in to the UT by evaporation of cloud ice [e.g., *Udelhofen and Hartmann*, 1995; *Su et al.*, 2006]. Other studies have, on the contrary, found that even the total evaporation of clouds cannot significantly contribute to the moistening. For example, *John and Soden* [2006] found the maximum IWP to be nearly an order of magnitude smaller than the maximum UTWV, and *Luo and Rossow* [2004] noted that the excessive amount of UTWV found in presence of clouds compared to clear-sky is around 50 times greater than the water contained in the cirrus. They explain the correlation of UTWV and IWP as a consequence of being transported to the UT by the same processes.

[5] Common to the previous studies is the use of column values for UTWV and cloud ice (IWP), typically between 200–500 mb [*Udelhofen and Hartmann*, 1995; *Luo and Rossow*, 2004] or 316–146 hPa [*Su et al.*, 2006; *John and Soden*, 2006]. The strong vertical gradient in water vapor mass weights such comparisons towards the lower part of the columns. The intrinsic difference in amount of water vapor within these altitude ranges approaches a factor 100, and the situation at the higher altitudes within the UT is therefore still uncertain.

[6] One reason that only column values have been used was the lack of reliable altitude resolved measurements of cloud ice and humidity in the UT. Profiles of radar reflectivity data from CloudSat and water vapor measurements from Aura/MLS are now publicly available. In this paper these datasets are used to study the fraction of water contained in cloud ice as a function of altitude within the tropical UT.

2. Data

[7] Both Aura and CloudSat are part of NASA's A-train satellite constellation. The measurements of the instruments follow similar orbital sub-tracks and are closely aligned in time, with a separation of around 10 minutes.

2.1. CloudSat

[8] CloudSat, launched in 2005, carries on board a cloud profiling radar (CPR) operating at 94 GHz in a nadir view [*Im et al.*, 2005]. Operational data, including geolocated profiles of radar reflectivity (dBZ) and IWC, are now available for release 4 (R04). Measurements from January to December 2007 have been included in this paper.

[1]Department of Radio and Space Science, Chalmers University of Technology, Göteborg, Sweden.

0094-8276/08/2008GL034305

Table 1. Averages for the CloudSat IWC Inversion Methods Described in the Text[a]

	Mean IWC (mg/m^3)		
Altitude (km)	CloudSat	LI00	MH97
9.7	10	9.6	10
12.0	6.3	3.8	5.2
14.3	1.5	0.50	0.88
16.6	0.052	0.012	0.022

[a]The values apply to the tropical region and are based on one month of data during Oct–Nov 2006.

[9] The radar reflectivity measurement only samples a specific particle size range, typically on the order of >100 μm. To account for the smaller particles the retrieval of IWC from the radar reflectivity measurements therefore has to include an assumption on the particle size distribution (PSD). This assumption can have a strong influence on the final result. To assess the systematic retrieval error coupled to the choice of inversion method, the global average of CloudSat IWC data over the tropical region is compared to two other methods; the dBZ to IWC parametrization by *Liu and Illingworth* [2000] (hereinafter referred to as LI00) and a dBZ parametrization based on the PSD of *McFarquhar and Heymsfield* [1997] (hereinafter referred to as MH97; see *Eriksson et al.* [2008] for details). Table 1 shows the resulting statistics for one month of observations during Oct–Nov 2006. The different methods are in good agreement at the lowest level, but they deviate rapidly with increasing altitude. At 100 hPa (highest level) the difference in average IWC reaches 400%. One source of the large differences between the official product and the dBZ conversions is probably the difference in basic methodology, column inversions contra point inversions. To assign a single value to represent the systematic uncertainty is problematic, but for the purpose of this paper it should be noted that the official CloudSat product throughout gives highest estimates. The random uncertainty is also difficult to estimate, but the large number of CloudSat observations ensures that even large random uncertainties have low importance for the averaged IWC.

2.2. Aura/MLS

[10] It is important that the water vapor measurements are as unaffected by cloud occurrences as possible to avoid introducing biases in the ice-fraction. Microwave limb-sounders show promising capabilities in sounding UT humidity with high vertical resolution and low cloud sensitivity [*Ekström et al.*, 2008]. Since Aura/MLS is part of the A-train, it is a suitable complement to the CloudSat observations in this study.

[11] Data of version 2.2 covering the same period as CloudSat, January to December 2007, have been considered, with an appropriate data screening as described by *Read et al.* [2007]. The estimated systematic and random retrieval uncertainties in the UT are 8–25% and 15–65%, respectively, with the best performance at higher altitudes.

3. Results

[12] The Aura/MLS water vapor and the CloudSat IWC data are averaged into 3° × 6° latitude-longitude gridboxes. Around 55,000 CloudSat profiles and 350 Aura/MLS profiles are included in each gridbox per year. The measurements are equally distributed over the gridboxes and cover similar volumes since both instruments follow the same orbital sub-track with global coverage. Selected vertical levels are chosen to coincide with the Aura/MLS retrieval levels in the pressure range 316–100 hPa, with the CloudSat altitudes converted to pressure levels using assimilated ECMWF altitude fields. The horizontal distributions of mass and ice-fraction are presented for four pressure levels; 316, 215, 147and 100 hPa (corresponding to 9.7, 12.0, 14.3 and 16.6 km), with data divided into semi-annual seasons. In this paper only figures for the Oct–Mar season are shown (figures for both seasons, Oct–Mar and Apr–Sep, are available in the auxiliary material).[1]

3.1. Ice Mass Density

[13] Semi-annual averages of IWC for the Oct–Mar season are shown in Figure 1. Figure 1 shows how the bulk of the ice mass is confined to the convectively active regions throughout the UT and TTL. In the upper TTL the occurrence of clouds with detectable amount of IWC becomes less frequent, allowing individual measurements of high IWC to dominate the grid-box averages causing a noisier appearance.

3.2. Water Vapor Mass Density

[14] In the gridbox averages the random uncertainty is reduced to $\leq$5% for all altitudes. The UTWV concentrations are converted to mass using the ideal gas law and an average tropical temperature profile based on ECMWF data.

[15] Figure 2 shows semi-annual UT water vapor mass fields for the same season as in Figure 1. The two lower altitudes resemble the corresponding cloud fields in Figure 1, with structures that follow the convective regions. A distinct change in structure appears between 215 and 147 hPa, and at the two upper levels belonging to the TTL region considerably smoother fields are observed.

3.3. Ice Fraction

[16] The ice-fraction f is calculated for each gridbox as the average mass of ice i divided by the sum of water vapor v and ice;

$$f = \frac{i}{i+v}. \quad (1)$$

3.3.1. Horizontal Distribution

[17] Horizontal fields for the Oct–Mar season are shown in Figure 3. The fraction of ice is very small at the lowest altitude, reaching 0.1 at the center of convective regions. Already 2 km higher up ice-fractions reach up to 0.25 and at 147 hPa ice even dominates in large parts of the convective regions. At the highest level, sporadic strong cloud signals result in local occasions of high ice-fractions that dominate the gridbox averages. Even though the magnitude varies, the structure of the horizontal distribution of ice-fraction is maintained at all levels.

3.3.2. Vertical Profiles

[18] The vertical profile of ice-fraction is presented for three different conditions of total water; dry, wet and medium. The gridboxes were categorized according the

[1]Auxiliary materials are available in the HTML. doi:10.1029/2008GL034305.

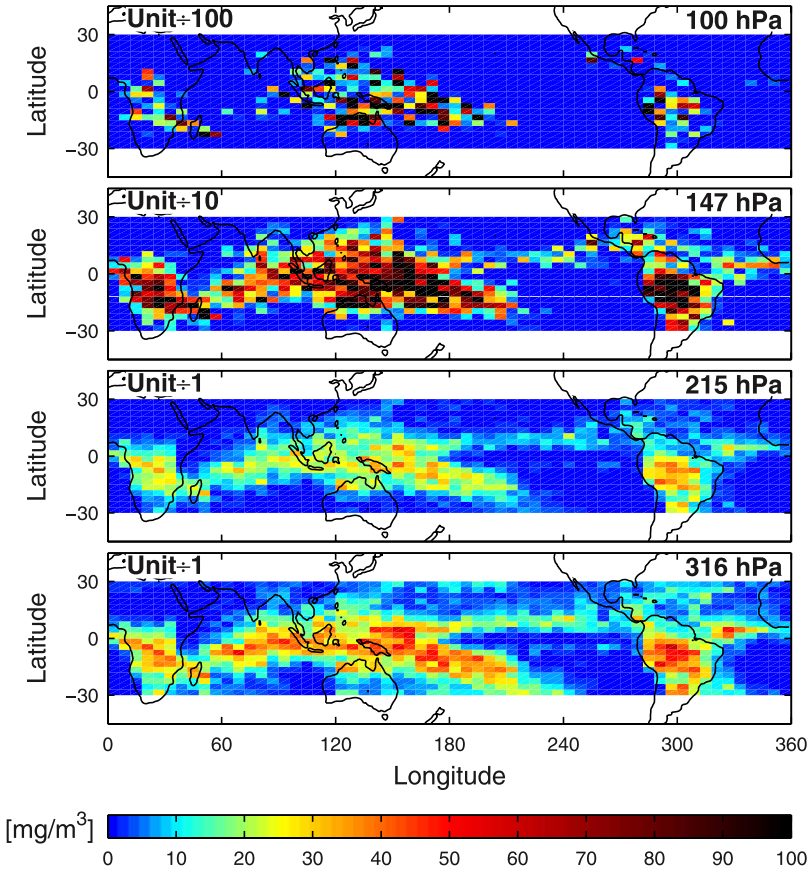

Figure 1. Horizontal distributions of average ice mass density in the upper troposphere. Data cover the months Oct–Mar 2007. In the top of each panel the pressure level and the unit scale factor are shown.

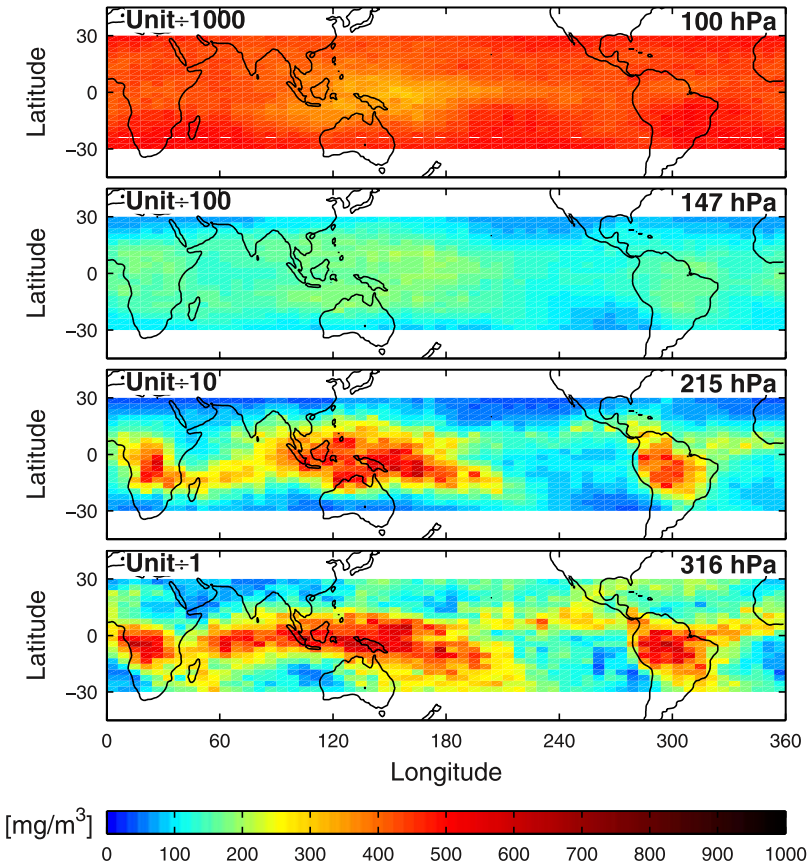

Figure 2. Horizontal distributions of average water vapor mass density in the upper troposphere. Data cover the months Oct–Mar 2007. In the top of each panel the pressure level and the unit scale factor are shown.

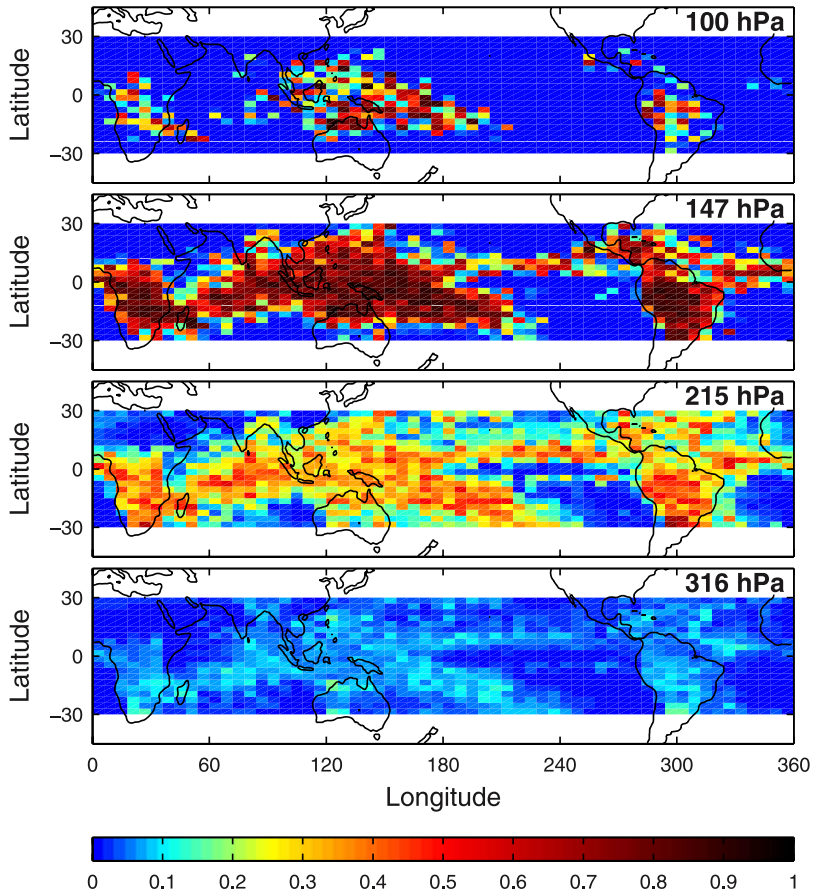

Figure 3. Fraction of ice mass over total mass H_2O at four pressure levels during the months Oct–Mar 2007.

their total water content at 316 hPa, where dry was defined as the 10% of the gridboxes with lowest water content, wet the highest 10% and medium the 10% about the median. Measurements within gridboxes of each category were averaged to create the vertical profiles in Figure 4. Altitudes coinciding with the seven Aura/MLS retrieval levels are included. Both the magnitude and peak altitudes of the ice-fraction increase with water content. In the wet regions the ice-fraction peaks above 147 hPa, i.e. in the TTL region, whereas the dry regions have their peak well below the TTL, 178–215 hPa. The medium category has a broader bulge, with maximum in between the two extremes.

[19] Figure 4 also show profiles for an estimated lowest ice-fraction. This estimate is based on the LI00 inversion for IWC data and Aura/MLS data increased by its systematic error estimate.

4. Discussion

[20] The distinct difference in horizontal structures seen in the water vapor fields between 215 and 147 hPa clearly marks the transition into the TTL, where convectional influence from below has decreased and zonal mixing has become more important. Below the TTL most of the total mass of water is found in the convectively active regions. This has also been found by previous observations of deep convection and UT clouds [e.g., *Soden and Fu*, 1995; *Wu et al.*, 2005]. Consistent with the column based studies of *Luo and Rossow* [2004] and *John and Soden* [2006] the fraction of ice is very small at these altitudes, while the congruent patterns of ice and water vapor illustrate the high correlation found by *Udelhofen and Hartmann* [1995] and *Su et al.* [2006]. This indicates that both vapor and cloud ice are transported up to the UT by the same processes. Outside the regions of deep convection the ice-fraction only reaches a few percent, and the maximum lies below the TTL.

[21] The fact that the horizontal structure of ice mass remains within the TTL is noteworthy. Over the convective

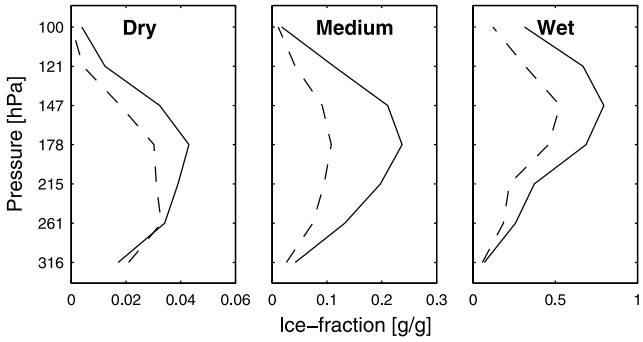

Figure 4. Vertical profiles of ice-fraction. The three panels show the average ice fraction profile for the three atmospheric states, dry, medium and wet, described in the text. Solid lines show results from the official CloudSat and Aura/MLS data, and dashed lines represent the estimated lowest ice-fraction obtained using the LI00 IWC retrieval.

regions the derived ice-fraction gives that cloud ice dominates the water content around 147 hPa. The exact magnitude of the ice-fraction is uncertain as the retrieval accuracies, particularly of the cloud ice inversion, are difficult to assess. The official CloudSat product gives comparably high IWC at the highest altitudes (Table 1) and the ice-fraction in the TTL can arguably have been overestimated. However, the estimated lowest ice-fraction, dashed lines in Figure 4, still gives ice-fractions of 45–70% for the wet profiles. In addition, the CloudSat data lack sensitivity to clouds consisting of exclusively small particles, but these clouds are expected to carry only a low portion of the ice mass and their influence would in any case be to increase the ice-fraction. Conclusively, cloud ice represents a significant portion of the total water content in the TTL above convective regions given the estimated uncertainties of the datasets, although the magnitude is uncertain.

[22] Even though the ice-fraction is locally significant in the TTL, the dissimilar patterns of cloud ice mass and water vapor suggest that the effective ice sublimation is small and only a low moistening effect is caused. If large parts of the ice would melt inside the TTL this should be discerned more clearly in the water vapor fields. This hypothesis has to be tested through model analysis, especially since the data examined here give no information on the dynamical processes or evolution of individual clouds in the TTL as the observations are ''snap-shots'' of the atmosphere. However, possible mechanisms, to explain the apparent low moistening of the TTL through lifting of cloud ice, are that the cloud particles have a relatively high sedimentation speed and are mainly found in parts of the atmosphere already close to water vapor saturation. Observations of relative humidity in this region give an average of 60–95%RHi [*Ekström et al.*, 2008].

[23] **Acknowledgments.** We thank Richard Austin and Dong Wu for valuable inputs on the data. NASA's CloudSat and Aura/MLS projects are acknowledged for providing the ice and water vapor data. Financial support was provided by the Swedish National Graduate School in Space Technology and the Swedish National Space Board.

References

Buehler, S. A., A. von Engeln, E. Brocard, V. O. John, T. Kuhn, and P. Eriksson (2006), Recent developments in the line-by-line modeling of outgoing longwave radiation, *J. Quant. Spectrosc. Radiat. Transfer*, *98*(3), 446–457, doi:10.1016/j.jqsrt.2005.11.001.

Ekström, M., P. Eriksson, W. G. Read, M. Milz, and D. P. Murtagh (2008), Comparison of satellite limb-sounding humidity climatologies of the uppermost tropical troposphere, *Atmos. Chem. Phys.*, *8*, 309–320.

Eriksson, P., M. Ekström, B. Rydberg, D. L. Wu, R. T. Austin, and D. P. Murtagh (2008), Comparison between early Odin-SMR, Aura MLS and CloudSat retrievals of cloud ice mass in the upper tropical troposphere, *Atmos. Chem. Phys.*, *8*, 1937–1948.

Im, E., C. Wu, and S. L. Durden (2005), Cloud profiling radar for the CloudSat mission, *IEEE Aerosp. Electron. Syst.*, *20*, 15–18.

John, V. O., and B. J. Soden (2006), Does convectively-detrained cloud ice enhance water vapor feedback?, *Geophys. Res. Lett.*, *33*, L20701, doi:10.1029/2006GL027260.

Lelieveld, J., et al. (2007), Stratospheric dryness: Model simulations and satellite observations, *Atmos. Chem. Phys.*, *7*, 1313–1332.

Liu, C.-L., and A. J. Illingworth (2000), Toward more accurate retrievals of ice water content from radar measurements of clouds, *J. Appl. Meteorol.*, *39*, 1130–1146.

Luo, Z., and W. B. Rossow (2004), Characterizing tropical cirrus life cycle, evolution, and interjection with upper-tropospheric water vapor using Lagrangian trajectory analysis of satellite observations, *J. Clim.*, *17*, 4541–4563.

McFarquhar, G. M., and A. J. Heymsfield (1997), Parameterization of tropical cirrus ice crystal size distributions and implications for radiative transfer: Results from CEPEX, *J. Atmos. Sci.*, *53*, 2187–2200.

Read, W. G., et al. (2007), Aura Microwave Limb Sounder upper tropospheric and lower stratospheric H2O and relative humidity with respect to ice validation, *J. Geophys. Res.*, *112*, D24S35, doi:10.1029/2007JD008752.

Soden, B. J., and R. Fu (1995), A satellite analysis of deep convection, upper-tropospheric humidity, and the greenhouse effect, *J. Clim.*, *8*, 2333–2351.

Su, H., W. G. Read, J. H. Jiang, J. W. Waters, D. L. Wu, and E. J. Fetzer (2006), Enhanced positive water vapor feedback associated with tropical deep convection: New evidence from Aura MLS, *Geophys. Res. Lett.*, *33*, L05709, doi:10.1029/2005GL025505.

Udelhofen, P. M., and D. L. Hartmann (1995), Influence of tropical cloud systems on the relative humidity in the upper troposphere, *J. Geophys. Res.*, *100*, 7423–7440.

Webster, C. R., and A. J. Heymsfield (2003), Water isotope ratios D/H, $^{18}O/^{16}O$, $^{17}O/^{16}O$ in and out of clouds map dehydration pathways, *Science*, *302*, 1742–1745.

Wu, D. L., W. G. Read, A. E. Dessler, S. C. Sherwood, and J. H. Jiang (2005), UARS/MLS cloud ice measurements: Implications for H_2O transport near the tropopause, *J. Atmos. Sci.*, *62*, 518–530.

M. Ekström and P. Eriksson, Department of Radio and Space Science, Chalmers University of Technology, Hörsalsvägen 11, SE-412 96 Göteborg, Sweden. (mattias.ekstrom@chalmers.se)